# Maximizing the efficiency of LCLCL-T Compensated Wireless Power Transfer Systems with independent-load Characteristics for charging applications in Smart Home

L. Yarmohammadi <sup>1</sup>, S.M.H. Hosseini <sup>1\*</sup>, J. olamaei <sup>1</sup>, and B. Mozafari <sup>2</sup>

\*Corresponding Author

Received 09 Aug. 2022

Received in revised form 12 Oct. 2022

Accepted 15 Nov. 2022

Type of Article: Research paper

Abstract- current study focuses on optimizing the efficiency of an LCLCL-T compensated topology in wireless power transfer systems with load-independent output current capability for battery charging. Wireless battery chargers play key devices in smart homes. To improve efficiency in these chargers, various compensated topologies are employed. In particular, the symmetric compensated LCLCL-T topology has been extensively used due to its inherent features, such as constant current output (CC), and high ability to absorb parasitic elements. However, one of the main deficits of this resonant compensation is decreased load regulation despite controlling the frequency, and on the other hand, its efficiency decreases owing to an increase in the circulating current. Therefore, in this study, the parameters of the proposed topology are reconfigured by adjusting the KW/KVA as an index to a reduction of voltage/current stresses on their elements without changing the specified system-level parameters, such as the system operating frequency, and specified CC output. Moreover, the circuit performance in the high-frequency response under different conditions is analyzed in detail, to optimize the system efficiency. Finally, the proposed system is simulated in PSIM to design the specific parameter values, the sample topology is also carried out. Analytical results show that the proposed compensation has the minimum output current fluctuation versus variations of the coupling coefficient and other parameters. Moreover, the analysis proves that, compared with the conventional design method, the proposed method improves the topology efficiency under various loads, especially under light loads.

*Keywords*: smart home, constant current application, wireless power transfer, optimization, parameter tuning method.

| N  | NOMENCLATURE  |  |  |  |  |
|--|---|--|--|--|--|
| BR   | ν   |  |  |  |  |
| $L_P$  | Secondary series resonant capacitor                           |  |  |  |  |
| $L_{S}$  | Primary leakage inductor                                      |  |  |  |  |
| $L_{\rm m}$  | Magnetizing inductor of transformer referred to primary       |  |  |  |  |
| $V_1$  | output voltage of the inverter                                |  |  |  |  |
| k  | coupling coefficient of the transformer                       |  |  |  |  |
| $I_{RL}$   | Load current  |  |  |  |  |
| $\omega_{re}$  | Base resonant frequency                                       |  |  |  |  |
| $\omega_{n,s}$   | normalized switching frequency                                |  |  |  |  |
| $Z_0$  | base characteristic impedance of network                      |  |  |  |  |
| $I_{on}$   | normalized output current                                     |  |  |  |  |
| $\alpha = L_2/L_1 \beta = L_3/L_1, \delta = L_4/L_1, \gamma = C_2/C_1, \tau = C_3/C_1$ | The ratio of resonance tank elements                          |  |  |  |  |
| $I_o$  | output current  |  |  |  |  |
| θ  | phase angle between the LCLCL-T input voltage and current     |  |  |  |  |
| $Q_{optimum}$  | the optimal Q function  |  |  |  |  |
| Romax  | maximum load resistance                                       |  |  |  |  |
| fs   | switching frequency   |  |  |  |  |
| $V_{i,rms}$  | RMS value of the fundamental harmonic of the RN input voltage |  |  |  |  |
| Iout   | Load current  |  |  |  |  |
| $R_{out}$  | Load resistance   |  |  |  |  |
| n  | transformer turn ratio  |  |  |  |  |

<sup>&</sup>lt;sup>1</sup> Department of Electrical Engineering, South Tehran Branch, Islamic Azad University, Tehran, Iran (e-mail: l\_yarmohammadi@azad.ac.ir, smhh110@azad.ac.ir, j\_olamaei@azad.ac.ir).

<sup>&</sup>lt;sup>2</sup> Department of Electrical Engineering, Science and Research Branch, Islamic Azad University, Tehran, Iran (e-mail: email:mozafari@srbiau.ac.ir).

| Q     | quality factor   |
|-------|--|
| ωsw   | switching frequency  |
| $R_L$ | equivalent AC resistance seen from the primary side of transformer |
| МРТВ  | the maximum power transmission basis index                         |

#### I.INTRODUCTION

ECENTLY, the wireless power transfer (WPT) Recently, the wheres point and explosed in various smart electronics devices home applications, from low-power electronics devices to high-power systems such as mobile robots [1,2], and electric Vehicles (EV) [3,4], respectively. In comparison with conventional plugged-in charging, the advantages of WPT systems are safety, portability, flexibility, and feeding without the user requirement [5]. The proper and effective operation of this device requires the use of a stable charging system with high-performance capability in terms of voltage fluctuation, which increases the life of batteries [6]. Some targets for designing an efficient WPT system are defined, as follows: 1) Improving power level [7]; 2) Increasing the power transfer distance [8]; 3) considerations between the transmitting and receiving sides to achieve a high coupling coefficient and misalignment tolerance [9]; and 4) consideration on coil geometry [10]. Therefore, according to these considerations, the appropriate WPT technologies can be designed for different applications, e.g. EV charging. In wireless charging technology, compensation topologies with constant output characteristics are an important issue. In this context, various topological techniques [11] and control strategies [12,13], are investigated to achieve a CC characteristic. Various control methods which are proper for WPT systems are used to regulate outputs under different load conditions [14-16]. High energy losses, dependence on sensors, and occupying a lot of space can be the major limitations of these strategies [17,18]. However, topological methods are a simpler controller design and cost-effective. One of the approaches is to apply a Resonant Network (RN) due to its considerable advantages [19]. RN is recognized as a considerable significant factor in improving the system efficiency and quality. It can be proved through the addition of two compensation circuits into the primary and secondary sides [20–21].

Presently, due to the simple and high-frequency response, two series/series resonance (S/S) and series/parallel resonance (S/P) topologies have the most attention for use in WPT systems. In [22], the load-independent output current and input impedance of the (S/S) and (S/P) compensations have been studied and compared. It has been investigated [22] that the S/S compensation can achieve both load-independent output current and zero input phase angle (ZPA) at a particular operating frequency. Therefore, S/S compensation is normally proper for current-source-output WPT systems.

However, the output current of the S/S compensation is inversely proportional to the mutual inductance of the WPT transformer, denoted as M. Moreover, when M varies, the output current also varies [23]. Moreover, series topology has good efficiency but suffers from poor load regulation even with frequency control [24]. In previous works, the merit and demerit of various third-order topologies such as the SS, SP, PS, and PP are discussed completely [25]. To improve the performance of the compensation network, many researchers have focused their attention on the advantageous high-order compensation topologies for their advantages [26], but, these researchers have little attention and focus on the coupling coefficient and other parameters of circuits for achieving high-efficiency systems.

On the other hand, according to [27], power transfer efficiency is related to the inverter part of a WPT system and it can be defined as the power inverter. Fig. 1, presents a typical WPT system with a series-series (SS) compensation topology.

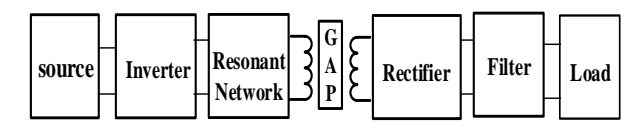


Fig. 1. A general structure of the WPT system block diagram.

In Fig. 1, the full bridge Inverter produces a square wave with quite a few harmonics. According to [28], by designing the compensation topologies as a passive bandpass filter, the harmonic components can be significantly attenuated. Several investigations have been performed on the analysis of harmonics of the inverter output in WPT systems [29-33]. In [29], eliminating the current harmonics by employing an LC as a low-pass filter is studied, but system efficiency is not the analysis in detail. By using an E-class rectifier in the high frequency (MHz) range for a WPT system, the THD of input voltage in an E-Class rectifier is decreased sufficiently in comparison with a conventional rectifier [30]. However, this report is only limited to the rectifier part. In [31], the authors investigated the reactive power levels for various compensation topologies. As a result, the LCC compensation was reported as a topology with high performance in terms of output reactive power. To improve the inverter output power of the WPT system, a Cascaded multi-level inverter is proposed in [32,33]. In these papers, the reduction of harmonics is discussed, but, the relationship between system efficiency and harmonic content of the inverter voltage is not investigated, in detail.

Owing to the above works of literature, in the current study, which is based on a mathematical method for tuning parameters proposed in [34], an identical compensation inductance of the LCLCL-T type is first established according to the essential parameters of the WPT system. This topology is the most similar topology to S/S compensation indirectly (transferring some of its reactive elements to the secondary part of the transformer). Without changing the specified systemlevel parameters, the resonant network is reconfigured by adjusting the ratio of the two compensation inductances of the proposed topology. Under these different combinations, the system characteristics such as current/voltage stress, and high-frequency response with respect to input current harmonics are carried out, in detail. LCLCL-T topology to determine an optimal value of the reactive components, which can enhance the system efficiency. The effectiveness of the proposed approach is assessed through simulations, and practical experiments, and compared with the conventional design method.

#### A. Contribution

This study elaborates on a mathematical method for achieving a Load-Independent Output Current. In comparison with the conventional design method, the proposed method improves the topology efficiency under various loads, especially under light loads.

In this paper, the parameters of the proposed topology are reconfigured by adjusting the KW/KVA as an index to a reduction of voltage/current stresses on their elements without changing the specified system-level parameters, such as the system operating frequency, and specified CC output. Due to prevent the increase in power losses and reduce the damage to the devices, the analysis of compensating topologies from the perspective of voltage and current stresses are important.

According to the above works of literature, this article has the merit of investigating the relationship between system efficiency and harmonic content of the inverter voltage. By adjusting the ratio of the two compensation inductances of the proposed topology, the system characteristics such as high-frequency response with respect to input current harmonics are carried out, in detail.

# B. Outlines

The structure of the rest of this article is as follows. In Section II, the theoretical analysis and design of an LCLCL-T are described, in detail. In Section III, the system Property Under these different combinations, such as voltage/current Stress, and high-frequency response, are discussed and compared to determine an optimal ratio of the reactive components, which can enhance the WPT system efficiency. In Sections IV, an evaluation of the efficiency of represented design methodology is carried out using contemporary feasible experiments.

## II.ANALYSIS AND DESIGN OF LCLCL-T COMPENSATED WPTS

A diagram of an LCLCL-T compensated WPTs is presented in Fig. 2. Proposed topology is the most similar structure to S/S compensation indirectly (transferring an LC to the secondary of the transformer). This topology comprises two inductors of  $L_1$  and  $L_2$ , which are in series with two capacitors  $C_1$  and  $C_2$ , respectively. Moreover,  $L_3$  is a parallel inductor with a T-composite. The proposed topology is the adaptable structure in terms of complete modeling of transformers instead of  $L_1$ ,  $L_2$ , and  $L_3$ . The leakage inductances of the transformer ( $L_p$  and  $L_s$ ) are used as components of the resonant network (RN)  $L_1$ , and  $L_2$  and primary-side magnetizing inductance ( $L_m$ ) as  $L_3$ . Therefore, leakage inductors and reactive components are decreased, resulting in minimal power losses and higher output efficiency.

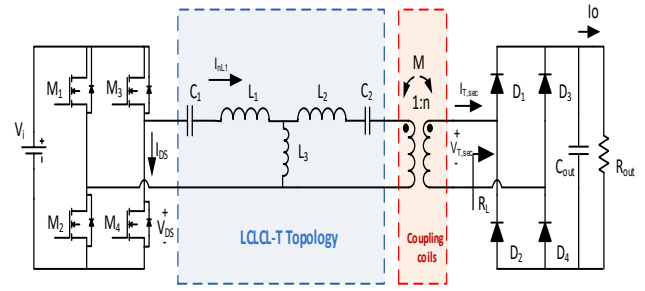


Fig. 2. LCLCL-T compensated WPT system for EV charging.

The full-bridge inverter (FBI) consists of four MOSFETs  $M_1$ - $M_4$  that is utilized to convert a DC-link voltage  $V_i$  to an AC square-wave voltage  $V_1$ . This voltage is a symmetric square Waveform of which amplitude is ideally equal to  $V_i$ . The fundamental harmonic analysis (FHA) for WPT systems is a general method for harmonic analysis in the resonant network (RN) [35]. The symmetric square wave can be expressed with Fourier series expansion as follows:

$$\begin{cases} V_{1}(\omega_{s}t) = \frac{a_{0}}{2} + \sum_{m=1,2,\dots}^{\infty} (a_{m}\cos(m\omega_{s}t) + b_{m}\sin(m\omega_{s}t)) \\ b_{m} = \frac{2}{\pi} \int_{0}^{\pi} V_{1}(\omega_{s}t)\sin(m\omega_{s}t)) d\omega_{s}t = \frac{4}{m\pi} \quad m = 1,3,\dots \end{cases}$$

where,  $\omega_s$  and m are is the switching frequency and harmonic indices, respectively. The zeroth harmonic  $(a_0)$  and Amplitudes of higher harmonics  $(a_m)$  is equal to zero for a square wave with a symmetry along time axis. Therefore, the Fourier series relation expansion of the output voltage can be resulted in:

$$V_1(t) = \frac{4V_i}{\pi} \sum_{n=1}^{\infty} \frac{1}{(2m-1)} \sin((2m-1) \omega_s t)$$
 (2)

where,  $\omega_s$  is the switching frequency. By operating the inverter at the resonant frequency of the circuit, the same phase of the output voltage and current is obtained. At this frequency, the network impedance generally includes the fundamental harmonic and higher harmonic

frequencies can be ignored. Therefore, the output voltage of the inverter is roughly defined as follows:

$$V_1(t) \approx V_1^{fundamental}(t) = \frac{4V_i}{\pi} \sin(\omega_s t)$$
 (3)

This approximation is more obvious, if the switching frequency is near the resonance frequency. By defining D as the steady state duty cycle, the output voltage of inverter  $V_I$  under a PWM control can be derived as:

$$V_1(t) = \frac{4V_i}{\pi} \sin(\omega_s t) \sin(\pi D) \tag{4}$$

The transformer is consist of a primary and secondary coil and Power is transferred from the primary to the secondary of its coils, the coupling coefficient of the transformer is considered as:

$$L_p/L_s \approx N_p^2/N_s^2 = \frac{1}{n^2}, \ k = M\sqrt{L_p \times L_s} \eqno(5)$$

Where L<sub>p</sub>, L<sub>s</sub>, and M are the leakage-inductance primary side, leakage-inductance secondary side, and mutual inductance of the transformer, respectively. By operating RN as a low-pass filter, the following RMS load output equations can be given [36]:

$$\begin{cases} V_{RL} = \frac{\pi\sqrt{2}}{4}V_1 \\ I_{RL} = \frac{\pi\sqrt{2}}{4}I_1 \end{cases}$$
 (6)

## C. LCLCL-T analysis

To obtain the output current expression of the proposed LCLCL-T and consider the above relationships, the equivalent circuit of the proposed topology can be simplified as Fig. 3.

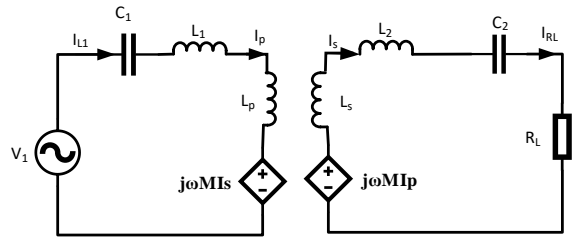


Fig. 3. Equivalent analytical circuit of the LCLCL-T topology. To start the design process via resonant conditions, the output current expression of the proposed topology, some basic parameters should be defined as:

1) The base resonant frequency, normalized switching frequency, the RN quality factor, and equivalent AC resistance seen from the primary side of transformer equivalent are defined as:

$$\omega_{\text{re}} = \frac{1}{\sqrt{L_1 C_{1,}}}, \, \omega_{\text{n,s}} = \frac{\omega_{\text{sw}}}{\omega_{\text{re}}}, \, Q = \frac{n^2 Z_0}{R_{\text{out}}}, \, R_L = \frac{8R_{\text{out}}}{n^2 \pi^2}$$
 (7)

In which  $\omega_{sw}$  is the switching frequency and n is the transformer turn ratio.

2) The base characteristic impedance of network, the RMS value of the fundamental harmonic of the RN input

voltage, and the normalized output current can be expressed as:

$$(Z_0 = \sqrt{\frac{L_1}{c_1}}), V_{i,rms} = \frac{2\sqrt{2} V_i}{\pi}, I_o = \frac{2\sqrt{2} I_{RL}}{\pi}, I_{on} = \frac{nI_o}{\frac{V_i}{Z_o}}(8)$$

3) The ratio of resonance tank elements is defined as:

$$\alpha = L_2/L_1$$

$$\beta = L_3/L_1, \delta = L_4/L_1, \gamma = C_2/C_1, \tau = C_3/C_1$$
 (9)

 $\alpha$  and  $\beta$  achieving will be explained in the next sections. This point should be noted that the basic capacitive and inductive are needed to create resonance conditions. Then, other components' relations can be derived according to the basic defined components. According to Kirchhoff's voltage and current laws, the expressions of the impedances can be derived as given in (9).

$$\begin{cases}
Z_p = s(L_p - M) + \frac{1}{sC_p}, \\
Z_s = s(L_s - M) + \frac{1}{sC_s}, \\
Z_M = sM
\end{cases}$$
(10)

$$Z_{M} = sM$$
Next, the  $R_{L}$  normalized current can be expressed as:
$$I_{on} = \frac{R_{L}Z_{M}}{R_{L}Z_{M} + Z_{S}Z_{M} + R_{L}Z_{p} + Z_{M}Z_{p}}$$
(11)

By writing the resonance network equations as well as altering the defined parameters (7-9), the normalized output current is illustrated as follows:

$$I_{on} = \frac{8}{\pi^2} \frac{j\gamma\beta\omega_n^3}{A_1 + jA_2} \tag{12}$$

In which,  $A_1$  and  $A_2$  are obtained as:

$$A_1 = 1 - (1 + \alpha \gamma + \beta + \beta \gamma)\omega_n^2 + (\alpha \gamma + \beta \gamma + \alpha \beta \gamma)\omega_n^4$$
(13)  
$$A_2 = \frac{8\gamma}{\pi^2 0} \left(\omega_n - (1 + \beta)\omega_n^3\right]$$
(14)

From (12), it has been clear that the topology behaves as load-independent if  $A_2$  is zero. Therefore, under this condition, the Normalized Operation Frequency ( $\omega_{n,s}$ ) under load- condition, is given as follows:

$$\omega_{n,s} = \frac{1}{\sqrt{1+\beta}} \tag{15}$$

Next, according to (15), the phase angle between the LCLCL-T input voltage and current is obtained as:

$$\theta = Arctg\left(\frac{-\pi^2 Q(1+\beta) - \gamma(\beta+\alpha)}{8\gamma(1+\beta)\sqrt{(1+\beta)}}\right)$$
 (16)

By considering the phase angle  $(\theta)$  equal to zero, it can be seen that the losses of the inverter switches are minimized. In this case, the relation among reactive

elements is expressed as:
$$\alpha = \frac{1+\beta-\beta\gamma}{\gamma}$$
(17)

Utilizing (15) and (17), the desired value of the LCLCL-T normalized output current can be resulted in:

$$I_{on}/_{\omega_n = \frac{1}{\sqrt{1+\beta}}, \ \alpha = \frac{1+\beta-\beta\gamma}{\gamma}} = \frac{-8\sqrt{(1+\beta)}}{j\pi^2\beta}$$
 (18)

In this state, the output current only depends upon  $(\beta)$ . Therefore, achieving the output current can be controlled by adjusting  $(\beta)$ . Moreover, higher design flexibility is one of the achievements of this feature.

### A. LCLCL-T design

The values of RN inductive/capacitance elements and their voltage/current range are the basic key to designing compensated WPT systems that lead to a reduction in voltage and current stresses and an increase in the capability of power transferring [37]. According to this concept, kVA/kW ratio is defined as the maximum power transmission basis (MPTB) index, which can be given as the following index:

$$MPTB = \frac{KVA}{KW} = \frac{\sum_{x=1}^{3} (V_{nLx} \times I_{nLx}) + \sum_{x=1}^{2} (V_{nCx} \times I_{nCx})}{\frac{I_{On}^{2}}{O}}$$
(19)

The normalized current and voltage relations of load-independent LCLCL-T components under condition is obtained as:

$$MPTB = \frac{16(1+\beta)\sqrt{1+\beta}}{\pi^2 \ Q \ \beta^2} + \frac{\pi^2 \ 2Q \ (\beta+\alpha)}{8 \sqrt{1+\beta}}$$
 (20)

As can be seen from (19), the MPTB value is the function of  $(\alpha, \beta, \text{ and } Q)$ . Given the dependence of Q on the load, it is found that Q is the only variable parameter throughout the circuit operation that changes the value of MPTB; therefore, the optimal Q function can be obtained as follows:

$$Q_{optimum} = \frac{8(1+\beta)}{\pi^2 \beta \sqrt{\beta + \alpha}}$$
 (21)

Using the optimum Q value, MPTB and the physical size of the circuit elements are minimized which can lead to the maximum power transfer, which is the objective of the proposed system. Accordingly, the following relationships can be obtained as the following:

transformer turn ratio: 
$$n = \frac{I_o \times R_{omax}}{V_i} \sqrt{\frac{1+\beta}{\beta+\alpha}}$$
 (22)

$$L_{1} = \frac{4}{\pi^{3}} \sqrt{\frac{\beta + \alpha}{1 + \beta}} \frac{V_{i}^{2}}{I_{0}^{2} R_{omax} f_{s} \beta}$$

$$C_{1} = \frac{\pi I_{0}^{2} R_{omax} \beta}{16 V_{i}^{2} f_{s} \sqrt{(\beta + \alpha)(1 + \beta)}}$$
(23)

$$C_1 = \frac{\pi l_0^2 R_{omax} \beta}{16 \, V_i^2 f_{\rm S} \sqrt{(\beta + \alpha)(1 + \beta)}} \tag{24}$$

Where  $R_{omax}$  is the maximum load resistance and  $f_s$  is the switching frequency.

#### III.PROCESS OF MAXIMIZING THE EFFICIENCY FOR THE

#### IV.LCLCL-T TOPOLOGY

Using the relationships obtained in the previous section, the values of  $L_2$ ,  $L_3$ , and  $C_2$  can be calculated. These parameters are a function of  $(\alpha, \beta, \text{ and } \gamma)$ . Furthermore, according to (4), all transformer parameters are expressed as functions of coupling coefficient. Table.I, the normalized current and voltage values of elements in conventional and under independent-load conditions. Therefore, in order to achieve the appropriate values of  $(\alpha, \beta, \text{ and } \gamma)$  values with respect to their current and voltage, the behavior of the circuit should be considered in the following scenarios.

#### A. Voltage and Current Stresses on the elements

The current, as well as voltage stresses on the reactive elements, are basic remarks while analyzing an RN compensated WPT structure because the increase in voltage/current stresses has an effect on power losses and can be damaged the equipment.

By choosing the appropriate values of the proposed circuit parameters, voltage and current stresses can be significantly reduced. Table I shows the values of voltage and current of components. It is clear that selecting the proper  $\beta$  can considerably decrease the voltage/current stress on the elements. The voltage/current parameters are directly related to the value of  $(\beta)$ . According to the previous section,  $L_1$  and  $L_2$  have a relation to Lp and Ls. Therefore, the possible value range of  $\beta$  should be related to the dimensions of the coils of the transformer. According to practical limitations, the values obtained at the 30 mm air gap for the proposed ferrite core in the laboratory, the value of 0.14 is appropriate for  $(\beta)$ . To investigate the relationship between the stress of the reactive elements and  $\beta$ , the list of base system parameters was selected, as Table II.

The frequency of 85 kHz was chosen due to its compatibility with the SAE J2954 standard of electric vehicle applications [38]. It is noteworthy that regulated voltage/current stresses on LCLCL-T elements under different  $(\beta)$  values, which are within independent-load conditions under the steady-state output circumstances, were presented and compared in Figure 4. According to fig. 4, the current and voltage stresses decrease with the  $\beta$ reduction.

TABLE I BASE PARAMETERS OF THE WPT SYSTEM

| symbols | parameters                | values  |
|---------|---------------------------|---------|
| Vi      | DC-link input voltage     | 31.5 V  |
| Fsw     | switching frequency       | 85 kHz  |
| Po      | Output power rating       | 170 W   |
| K       | Coupling coefficient      | 0.14    |
| Lp      | Primary coil inductance   | 62.4 µH |
| Ls      | Secondary coil inductance | 62.4 µH |

TABLE II

NORMALIZED CURRENT AND VOLTAGE VALUES OF ELEMENTS IN CONVENTIONAL AND INDEPENDENT-LOAD CONDITIONS

| NORMALIZED CURRENT AND VOLTAGE VALUES OF ELEMENTS IN CONVENTIONAL AND INDEPENDENT-LOAD CONDITIONS. |  |  |  |  |  |  |  |
|--|--|--|--|--|--|--|--|
| Normalized I & V of components   | Conventional condition   | independent-load condition   |  |  |  |  |  |
| $I_{nL1} = I_{nC1} = \frac{I_{L1}}{\frac{V_i}{Z_0}} = \frac{I_{C1}}{\frac{V_i}{Z_0}}$              | $\frac{2\sqrt{2}}{\pi} \frac{\left[\frac{-8\gamma\omega_n^2}{\pi^2 Q}\right] + j\left[\omega_n - \gamma(\beta + \alpha)\omega_n^3\right]}{A_1 + jA_2}$ | $\frac{16\sqrt{2}\left(1-\beta\right)}{\pi^3 Q\beta^2}$                                    |  |  |  |  |  |
| $I_{nL2} = I_{nC2} = \frac{I_{L2}}{\frac{V_i}{Z_0}} = \frac{I_{C2}}{\frac{V_i}{Z_0}}$              | $\frac{2\sqrt{2}}{\pi} \frac{-j\gamma\beta\omega_n^3}{A_1 + jA_2}$   | $\frac{2\sqrt{2}\sqrt{(1+\beta)}}{\pi\beta}$   |  |  |  |  |  |
| $I_{nL3} = \frac{I_{L3}}{\frac{V_i}{Z_0}}$   | $\frac{2\sqrt{2}}{\pi} \frac{\left[\frac{-8\gamma\omega_n^2}{\pi^2Q}\right] + j\left[\omega_n - \gamma\alpha\omega_n^3\right]}{A_1 + jA_2}$            | $\frac{2\sqrt{2}\sqrt{1+\beta}}{\pi\beta}\sqrt{(\frac{8\sqrt{1+\beta}}{\pi^2Q\beta})^2+1}$ |  |  |  |  |  |
| $V_{nL1} = \frac{V_{L1}}{V_i}$   | $\frac{2\sqrt{2}}{\pi} \frac{(\gamma(\beta+\alpha)\omega_n^4 - \omega_n^2) - j\frac{8\gamma\omega_n^3}{\pi^2Q}}{A_1 + jA_2}$                           | $\frac{16\sqrt{2}\sqrt{1+\beta}}{\pi^3 Q\beta^2}$  |  |  |  |  |  |
| $V_{nL2} = \frac{V_{L2}}{V_i}$   | $\frac{2\sqrt{2}}{\pi} \frac{(\gamma \beta \alpha \omega_n^4)}{A_1 + jA_2}$  | $\frac{2\sqrt{2}\alpha}{\pi\beta}$   |  |  |  |  |  |
| $V_{nL3} = \frac{V_{L3}}{V_i}$   | $\frac{2\sqrt{2}}{\pi} \frac{(\gamma \beta \alpha \omega_n^4 - \beta \omega_n^2) - j \frac{8\gamma \beta \omega_n^3}{\pi^2 Q}}{A_1 + jA_2}$            | $\frac{2\sqrt{2}}{\pi}\sqrt{(\frac{8\sqrt{1+\beta}}{\pi^2 Q\beta})^2+1}$                   |  |  |  |  |  |
| $V_{nc1} = \frac{V_{c1}}{V_i}$   | $\frac{2\sqrt{2}}{\pi} \frac{(1 - \gamma(\alpha + \beta)\omega_n^2) + j\frac{8\gamma\omega_n}{\pi^2 Q}}{A_1 + jA_2}$                                   | $\frac{16\sqrt{2}}{\pi^3 Q} \frac{(1+\beta)\sqrt{1+\beta}}{\beta^2}$                       |  |  |  |  |  |
| $V_{nC2} = \frac{V_{C2}}{V_i}$   | $\frac{2\sqrt{2}}{\pi} \frac{(\beta \omega_n^2)}{A_1 + jA_2}$  | $\frac{2\sqrt{2}(\beta+\alpha)}{\pi\beta}$   |  |  |  |  |  |

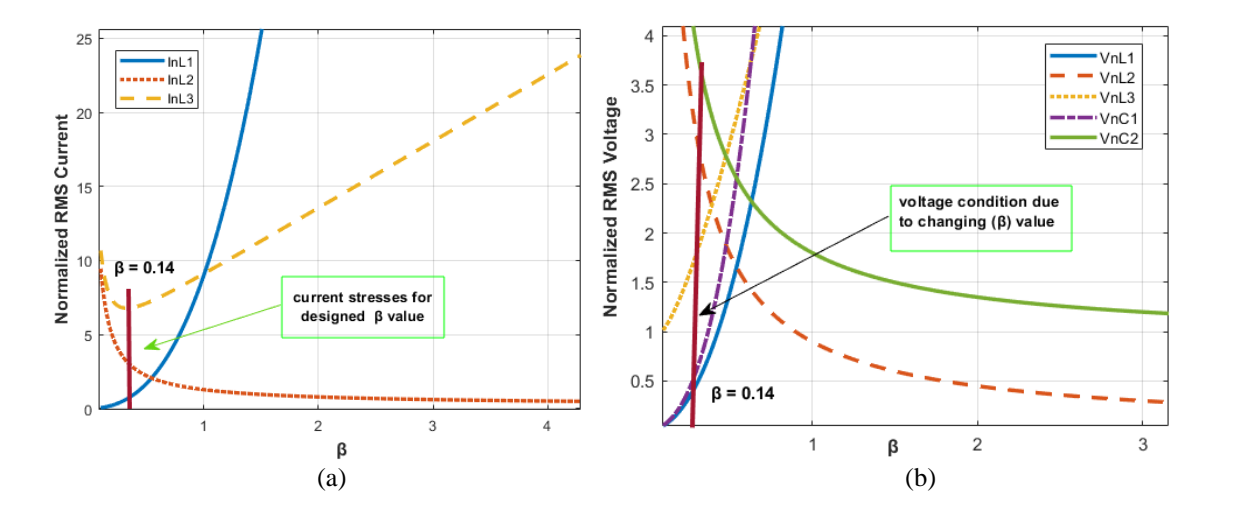


Fig. 4. Normalized voltage and current stresses on the LCLCL-T elements versus  $\beta$ . (a) Currents; (b) voltages.

## B. High-Order Harmonic Suppression

According to the discussion in the previous sections, among the functions of compensators is damping the leakage inductances of the transformer and also by acting as a filter, removing the high frequencies. Therefore, this

issue weakens the harmonic components [28]. Based on the previous analysis, reconfigurable parameters of the LCLCL-T for different  $(\beta)$  are calculated in table III.

TABLE III
CALCULATED RECONFIGURABLE PARAMETERS OF THE
LCLCL-T WPT COMPENSATED TOPOLOGY

| EOLOL I WI I COMI ENSATED TO OLOGI |                |                |               |                |  |  |
|------------------------------------|----------------|----------------|---------------|----------------|--|--|
| parameters                         | $\beta = 0.14$ | $\beta = 0.33$ | $\beta = 0.5$ | $\beta = 0.75$ |  |  |
| L1 (μH)                            | 62.4           | 26.45          | 17.46         | 11.64          |  |  |
| L2 (µH)                            | 62.4           | 26.45          | 17.46         | 11.64          |  |  |
| L3 (µH)                            | 8.74           | 26             | 8.73          | 8.73           |  |  |
| C1 (nF)                            | 49.3           | 99.63          | 1.34          | 17.2           |  |  |
| C2 (nF)                            | 49.3           | 99.63          | 1.34          | 17.2           |  |  |
| n                                  | 2.2            | 2.2            | 2.2           | 2.2            |  |  |

By substituting (20) in (11), and using the parameters listed in Table II, the amplitudes of  $I_{00}$  under different  $\beta$  are presented in Fig. 5. Because the inverter output ( $V_i$ ) includes only odd harmonics, and the higher-harmonic are ignorable; therefore, in fig 5, only the fundamental (85 kHz), third (255 kHz), and fifth (425 kHz) harmonics are considered. It can be seen, that the independent-load condition can always be obtained at the specified resonant frequency (85 kHz) with respect to  $\beta$ .

In addition, to verify the above analysis, under the same calculation conditions as above, comparative simulations were performed using the PSIM 9.1 software, as shown in Fig. 6. Furthermore, the fast Fourier transform (FFT) tool was used to analyze the input current  $I_{\rm in}$ . The fundamental harmonic amplitudes of  $I_{\rm in}$  are almost unchanged, whereas those of the third and fifth harmonics decrease as  $\beta$  increases. Hence, for higher performance, the selected  $\beta$  value should be as large as possible.

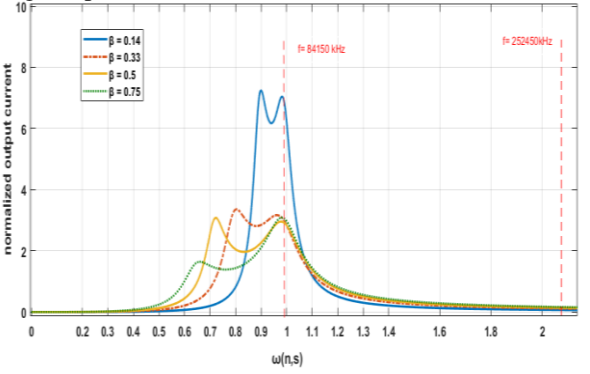


Fig. 5. Frequency-response characteristic of the LCLCL-T structure under different  $\beta$  values.

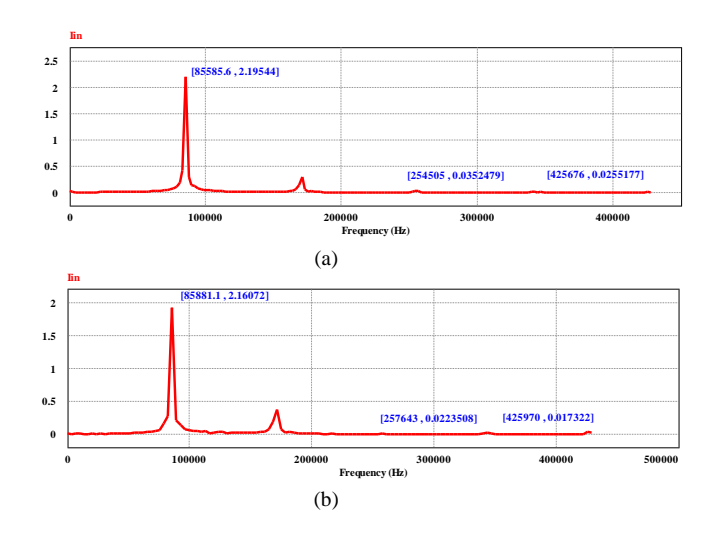


Fig. 6. PSIM simulation results of Iin harmonic under different  $\beta$ . (a)  $\beta = 0.14$ . (b)  $\beta = 0.33$ .

#### IV. EXPERIMENTAL VERIFICATION

#### A. Practical Result

To verify the above theoretical analysis and comparison, a 170W practical sample of the LCLCL-T topology was built, as shown in Fig. 6. In this setup, the main system parameters such as  $V_i,\ f_{sw},\$ and  $I_{RL}$  are consistent with those listed in Table II. The output power at 20–50 mm in a U-shaped transformer is transmitted to load 30  $\Omega.$  With the 30mm air gap and the windings 17 and 54 (38AWG Litz-wire) that turn onto cores, proper values of the proposed topology are obtained. The practical parameters with respect to ( $\beta=0.14$ ) were measured in laboratory, as listed in Table III. Four MOSFETs IRFP150 and four Schottky diodes MBR20100 are chosen as the FB inverter and rectifier, respectively. Micro ATmega32A was used to control the switches of the WPT system.

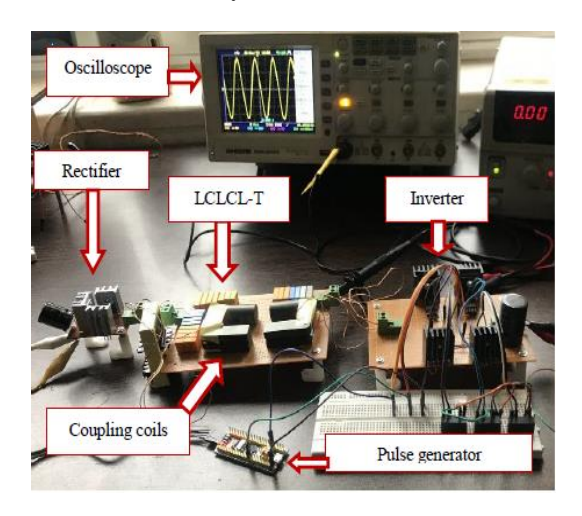


Fig. 7. Experimental prototype of an LCLCL-T.

The practical and simulation graphs at maximum load are indicated in Figure 7. It can be seen that the input current is in phase with the voltage across the power MOSFET  $M_3$ . According to Fig. 8, The ZVS realization for switches and the maximum coherence of the transformer output voltage and current result in minimal power loss of rectifier. In the output resistance condition, the output current is about 2.1A and the efficiency is 90%.

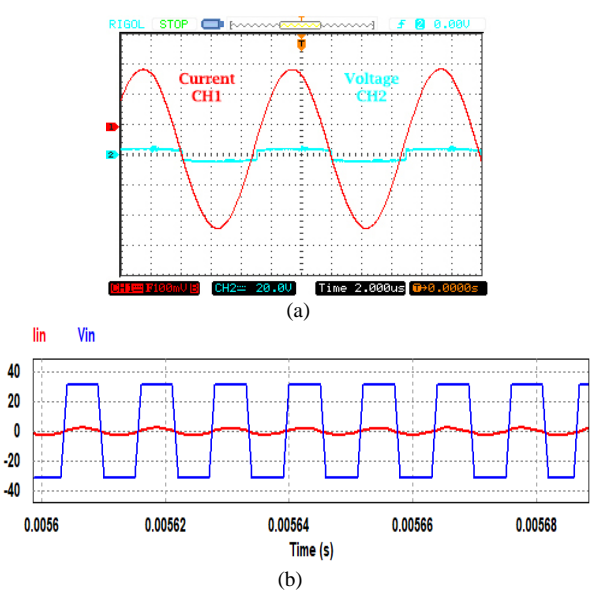


Fig. 8. LCLCL-T waveforms of input current and voltage at the maximum load. (a) experimental result (b) simulation.

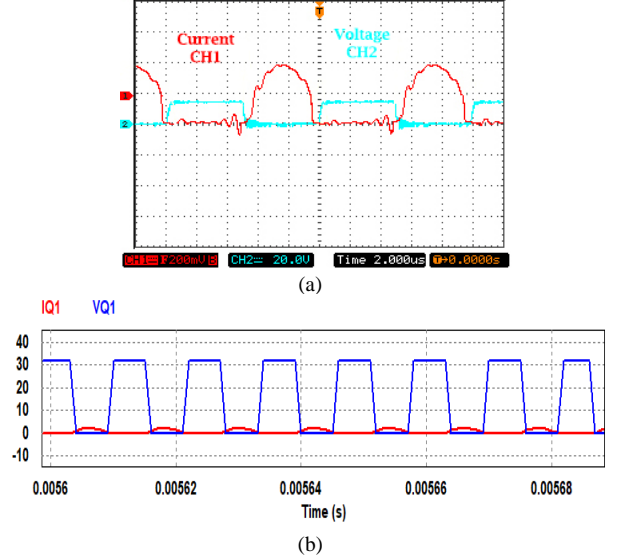


Fig. 9. LCLCL-T waveforms of voltage across switches and current through it.at the maximum load. (a) experimental result (b) simulation.

The output power,  $P_{out}$ , and efficiency,  $\eta$ , are calculated versus load variations by using:  $\eta = \frac{P_{out}}{P_{in}} = \frac{I_o^2 \times R_{out}}{V_i \times I_i}$ 

$$\eta = \frac{P_{out}}{P_{in}} = \frac{I_o^2 \times R_{out}}{V_i \times I_i} \tag{25}$$

The overall efficiency of the prototype is measured via a power meter versus the output power transfer, at maximum load condition, as illustrated in Fig. 9. This diagram shows the LCLCL-T optimal efficiency for different performance powers. Moreover, the current decreases with the load power, and it leads to the maintenance of increased converter effectiveness over the extensive fluctuations of generated power.

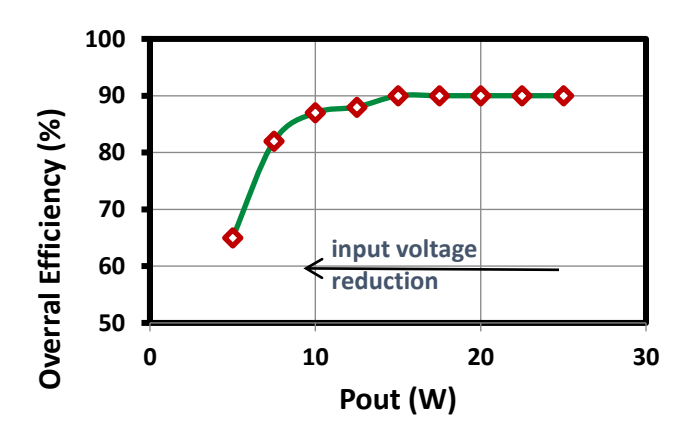


Fig. 10. Experimental efficiency of the system in various loads.

# B. Discussion and Comparison

To evaluate and verify the effectiveness of the proposed technique over the conventional approach to designing a load-independent output current topology for wireless power transfer (WPT) systems, the LCLCL-T in immittance mode and an S/S topology in the conventional approach presented in [18] are compared. Under the same comparative conditions, the following can be deduced: (1) one of the main deficits of S/S resonant compensation is decreased load regulation despite controlling the frequency [39]. However, the protection from short-circuit is achieved through LCLCL-T. Also, it is associated with inherent constant current characteristics under immittance circumstances, which leads to the elimination of deficits of the major S/S compensation in the process of light-load regulation. The results obtained at 1% of the full load are evidence to prove this case. (2) According to [18], efficiency is almost linearly decrease with the increase of the load. Therefore the expresses of that paper have indicated that efficiency is dependent on the load and efficiency is around 88% ~ 66% in operating frequency. Therefore, in a conventional mode for achieving maximum efficiency, it is assumed that proper frequency tracking is performed by complex control methods. However, in the method discussed in this paper, obtaining the  $Q_{optimum}$ , reducing the physical dimensions of the circuit, and increasing the efficiency have been achieved.

The comparative points mentioned above show that the IPRN topologies are superior in terms of load regulation, efficiency improvement based on the optimal quality factor, and other parameters of systems.

#### V. CONCLUSION AND FUTURE WORKS

In current study, a mathematical technique is proposed to adjust the parameters of the LCLCLC-T compensated topology in wireless power transfer systems with loadindependent output current capability for battery charging. Assuming that the basic parameters are established at the system level, the LCLCL-T topology was reconstructed by adjusting the ratio of compensating reactive elements. Therefore, the current/voltage of the primary and secondary sides of the transformer can be adjusted to create different system properties. The analyses under different parameters were conducted and an optimum reactive component ratio was investigated with high efficiency as the basic remark. Moreover, the circuit performance in the high-frequency response under different conditions is analyzed, to optimize the system efficiency. A practical setup was configured to validate the simulation results to design the specific parameter values. This hardware prototype ferrite-core was built with 90% efficiency at the coupling coefficient of 0.14 and 30mm air-gap. The analysis proves that, compared with the conventional design method, the proposed method improves the topology efficiency under various loads. The selection of other models of transformer coils and the analysis of core losses and copper losses of the LCLCL-T topology to improve the efficiency of WPT system to battery chargers applications are few topics suggested for future research.

## REFERENCES

- [1] Liu, H.; Huang, X.; Tan, L.; Guo, J.; Wang, W.; Yan, C.; Xu, C." Dynamic Wireless Charging for Inspection Robots Based on Decentralized Energy Pickup Structure". IEEE Trans. Ind. Inform. 2018, 14, 1786–1797.
- [2] Zhang, Y.; Tian, G.; Lu, J.; Zhang, M.; Zhang, S."Efficient Dynamic Object Search in Home Environment by Mobile Robot: A Priori Knowledge-Based Approach". IEEE Trans. Veh. Technol. 2019, 68, 9466–9477.
- [3] Huang, S.; Lee, T.; Li, W.; Chen, R."Modular On-Road AGV Wireless Charging Systems Via Interoperable Power Adjustment". IEEE Trans. Ind. Electron. 2019, 66, 5918–5928.
- [4] Siroos, A.; Sedighizadeh, M.; Afjei, E.; Fini, A.S." Comparison of different controllers for wireless charging system in AUVs". In Proceedings of the 2022

- 13th Power Electronics, Drive Systems, and Technologies Conference (PEDSTC Tehran, Iran, 1–3 February 2022; pp. 155–160.
- [5] Tang, Y.; Chen, Y.; Madawala, U.K.; Thrimawithana, D.J.; Ma, H. "A New Controller for Bidirectional Wireless Power Transfer Systems". IEEE Trans. Power Electron. 2018, 33, 9076–9087.
- [6] Esmaeil, J.; Salehizadeh, M.R.; Rahimikian, A."Optimal control of the power ramp rate with flicker mitigation for directly grid connected W.
- [7] Zhang, S. C. Wong, C. K. Tse, and Q. Chen, "Design for efficiency optimization and voltage controllability of series-series compensated inductive power transfer systems," *IEEE Trans. Power Electron.*, vol. 29, no. 1, pp. 191–200, Jan. 2014. wind turbines".
- [8] S. Samanta and A. K. Rathore, "Analysis and design of load independent ZPA operation for P/S, PS/S, P/SP, and PS/SP tank networks in IPT applications," *IEEE Trans. Power Electron.*, vol. 33, no. 8, pp. 6476–6482, Aug. 2018.
- [9] W. Zhang, J. C. White, R. K. Malhan, and C. C. Mi, "Loosely coupled transformer coil design to minimize EMF radiation in concerned areas," IEEE Trans. Veh. Technol., vol. 65, no. 6, pp. 4779–4789, Jun. 2016.
- [10] Barman, S. D., Reza, A. W., Kumar, N., Karim, M. E., & Munir, A. B. (2015). "Wireless powering by magnetic resonant coupling: Recent trends in wireless power transfer system and its applications," Renewable and Sustainable energy reviews, 51, 1525-1552.
- [11] Hou, J.; Chen, Q.; Zhang, Z.; Wong, S.; Tse, C.K." Analysis of Output Current Characteristics for Higher-Order Primary Compensation in Inductive Power Transfer Systems". IEEE Trans. Power Electron. 2018, 33, 6807–6821.
- [12] **Li**, Y., Sun, W., Zhu, X., & Hu, J. (2021). A hybrid modulation control for wireless power transfer systems to improve efficiency under light-load conditions. *IEEE Transactions on Industrial Electronics*, 69(7), 6870-6880.
- [13] Huang, Z.; Lam, C.; Mak, P.; Martins, R.P.d.S.; Wong, S.; Tse, C.K. "A Single-Stage Inductive-Power-Transfer Converter for Constant-Power and Maximum-Efficiency Battery Charging". IEEE Trans. Power Electron. 2020, 35, 8973–8984.
- [14] S. S. Lourdusami and R. Viaramani, "Analysis, design and experimentation of series-parallel LCC resonant converter for constant current source," IEICE Electron. Exp., vol. 11, no. 17, pp. 1–12, Aug. 2014.
- [15] F. Duan, M. Xu, X. Yang, and Y. Yao, "Canonical model and design methodology for LLC DC/DC converter with constant current operation capability under shorted load," IEEE Trans. Power Electron., vol. 31, no. 10, pp. 6870–6883, Oct. 2016.
- [16] Y. Li, Q. Xu, T. Lin, J. Hu, Z. He, and R. Mai, "Analysis and Design of Load-Independent Output

- Current or Output Voltage of a Three-Coil Wireless Power Transfer System," in IEEE Transactions on Transportation Electrification, vol. 4, no. 2, pp. 364-375, June 2018.
- [17] Salehizadeh, M. R., Koohbijari, M. A., Nouri, H., Taşcıkaraoğlu, A., Erdinç, O., & Catalao, J. P. (2019). Bi-objective optimization model for optimal placement of thyristor-controlled series compensator devices. Energies, 12(13), 2601.
- [18] R. Naghash, S. M. M. Alavi and S. E. Afjei, "Robust Control of Wireless Power Transfer Despite Load and Data Communications Uncertainties," in IEEE Journal of Emerging and Selected Topics in Power Electronics, vol. 9, no. 4, pp. 4897-4905, Aug. 2021.
- [19] B. E. Jamakani, E. Afjei, and A. Mosallanejad, "A Novel Triple Quadrature Pad for Inductive Power Transfer Systems for Electric Vehicle Charging," 2019 10th International Power Electronics, Drive Systems and Technologies Conference (PEDSTC), 2019, pp. 618-623.
- [20] Zhang and C. C. Mi, "Compensation topologies of high-power wireless power transfer systems," IEEE Trans. Vehicular Tech., vol. 65, no. 6, pp. 4768–4778, July. 2016.
- [21] A. Ramezani, S. Farhangi, H. Iman-Eini, B. Farhangi, R. Rahimi, G. R. Moradi, "Optimized LCC-Series Compensated Resonant Network for Stationary Wireless EV Chargers," IEEE Trans. on Industrial Electronics, vol. 66, no. 4, pp. 2756–2765, April 2019.
- [22] W. Zhang, S. C. Wong, C. K. Tse, and Q. Chen, "Load-independent duality of current and voltage outputs of a series- orparallel-compensated inductive power transfer converter withoptimized efficiency," IEEE J. Emerg. Sel. Topics in Power Electron.,vol. 3, no. 1, pp. 137–146, Mar. 2015.
- [23] X. Qu, W. Zhang, S. C. Wong, and C. K. Tse, "Design of a current-source-output inductive power transfer LED lighting system," IEEE J. Emerg. Sel. Topics in Power Electron., vol. 3, no. 1, pp.306–314, Mar. 2015.
- [24] V. J. Brusamarello, Y. B. Blauth, R. de Azambuja, I. Muller and F. R. de Sousa, "Power Transfer With an Inductive Link and Wireless Tuning," in *IEEE Transactions on Instrumentation and Measurement*, vol. 62, no. 5, pp. 924-931, May 2013.
- [25] Y. Yao, Y. Wang, X. Liu, F. Lin, and D. Xu, "A novel parameter tuning method for a double-sided LCL compensated WPT system with better comprehensive performance," IEEE Trans. Power Electron., vol. 33, no. 10, pp. 8525–8536, Oct. 2018.
- [26] Daniel Thenathyalan and Joung-HU park, "Highorder resonant converter topology with extremely lowcoupling contactless," IEEE Trans. on Power Electronics., vol. 31, no. 3, pp. 2347-2361, march. 2016.
- [27] Seyit Ahmet Sis, Hakan Akca, "Maximizing the efficiency of wireless power transfer systems with an optimal duty cycle operation," AEU-International

- Journal of Electronics and Communications. vol. 116, pp. 153081, March. 2020.
- [28] H. Zeng, S. Yang, and F. Z. Peng, "Design consideration and comparison of wireless power transfer via harmonic current," IEEE Trans. Power Electron., vol. 32, no. 8, pp. 5943–5952, Aug. 2017.
- [29] Xia C, Chen R, Liu Y, Liu L, Chen G., "Inhibition of current harmonics in LCL/LCC wireless power transfer system," In: 2017 IEEE PELS workshop on emerging technologies: wireless power transfer, WoW 2017. Institute of Electrical and Electronics Engineers Inc.; 2017.
- [30] Liu M, Fu M, Ma C., "Low-harmonic-contents and high-efficiency class e fullwave current-driven rectifier for megahertz wireless power transfer systems," IEEE Trans Power Electron 2017; 32(2):1198–209.
- [31] Luo S, Li S, Zhao H., "Reactive power comparison of four-coil, LCC and CLC compensation network for wireless power transfer," In: 2017 IEEE PELS workshop on emerging technologies: wireless power transfer, WoW 2017. Institute of Electrical and Electronics Engineers Inc.; 2017. p. 268–71.
- [32] Li Y, Mai R, Yang M, He Z., "Cascaded multi-level inverter based IPT systems for high power applications," J Power Electron 2015; 15(6):1508–16.
- [33] Li Y, Mai R, Lu L, He Z, Liu S., "Harmonic elimination and power regulation based five-level inverter for supplying IPT systems," In: IEEE WoW 2015 IEEE PELS workshop on emerging technologies: wireless power, proceedings. Institute of Electrical and Electronics Engineers Inc.; 2015
- [34] L. Yarmohammadi, S. M. H. Hosseini, J. Olamaei, and B. Mozafari, "A Load-Independent Output Current Method for Wireless Power Transfer Systems with Optimal Parameter Tuning," Sustainability, vol. 14, no. 15, p. 9391, Jul. 2022.
- [35] Y. Chen, H. Zhang, S. Park, and D. Kim, "A switching hybrid LCC-S compensation topology for constant current/voltage EV wireless charging," IEEE Access., vol.7, pp.133924–133935, Sept. 2019.
- [36] R. L. Steigerwald, "A comparison of half-bridge resonant converter topologies," IEEE Trans. Power Electron., vol. 3, no. 2, pp. 174–182, Apr. 1988.
- [37] M. Borage, K. V. Nagesh, M. S. Bhatia, and S. Tiwari, "Resonant immittance converter topologies," IEEE Trans. Ind. Electron., vol. 58, no. 3, pp. 971–978, Mar. 2011.
- [38] J.T. Boys, G.A. Covic, "The Inductive Power Transfer Story at the University of Auckland," IEEE Circuit Syst. Mag., vol. 15, pp. 6 27, 2015.
- [39] Kim, M.; Kim, J.; Lee, B. Adjustable frequency—duty-cycle hybrid control strategy for full-bridge series resonant converters in electric vehicle chargers. IEEE Trans. Ind. Electron. 2014, 61,